ChemPubSoc Europe

DOI: 10.1002/cphc.201900289

CHEMPHYSCHEM Communications

Observation of Photoelectron Circular Dichroism Using a Nanosecond Laser

Alexander Kastner,[a] Tom Ring,[a] Hendrike Braun,[a] Arne Senftleben,[a] and Thomas Baumert*[a]

Photoelectron circular dichroism (PECD) is a fascinating phenomenon both from a fundamental science aspect but also due to its emerging role as a highly sensitive analytic tool for chiral recognition in the gas phase. PECD has been studied with single-photon as well as multi-photon ionization. The latter has been investigated in the short pulse limit with femtosecond laser pulses, where ionization can be thought of as an instantaneous process. In this contribution, we demonstrate that multi-photon PECD still can be observed when using an ultra-violet nanosecond pulse to ionize chiral showcase fenchone molecules. Compared to femtosecond ionization, the magnitude of PECD is similar, but the lifetime of intermediate molecular states imprints itself in the photoelectron spectra. Being able to use an industrial nanosecond laser to investigate PECD furthermore reduces the technical requirements to apply PECD in analytical chemistry.

Chiral recognition in the gas phase with the help of electromagnetic radiation is an emerging research area as an interaction-free environment allows to study intrinsic chiral response.

In the last few years for instance fully coherent microwave three-wave mixing schemes,[1] Coulomb explosion imaging for direct absolute configuration determination,[2] circular dichroism (CD) in all-optical high-harmonic spectroscopy[3] as well as CD in ion yield[4] have been developed.

When chiral molecules are ionized by circularly polarized light, a forward-backward asymmetry in the photelectron emission direction with respect to the light propagation direction was predicted by theory.[5] This effect arises in the electric dipole approximation and was first observed experimentally using single-photon ionization.[6] The forward-backward asymmetry is known as photoelectron circular dichroism[7] (PECD) and typically exhibits large magnitudes with experimental values as high as 37%.[8] The origin of PECD lies in the quantum interference of outgoing partial waves.[9] As PECD has been observed for single-photon ionization out of an achiral core-shell orbital, it has been interpreted as being mainly a final state effect.[7,10] Measuring PECD has been boosted by techniques capturing the full photoelectron momentum distribution such as velocity map imaging (VMI)[11] or a recently developed stereo-electron detector.[12] Recently, single-photon PECD[13,14] highlighting in addition the relevance for astrophysical research[15] has been reviewed.

Note that ionization with a single photon is independent on the temporal structure of the light. At ultra-violet up to infrared wavelengths, several photons are necessary for ionization and the temporal structure becomes very important. Especially, the ionization probability rises steeply with intensity which is inversely proportional to the duration of light pulses. However, intermediate resonances can be populated and enhance the ionization yield. When intermediate states are populated, the question arises whether the internal dynamics of the molecule might influence the PECD signature. For femtosecond (fs) pulses, ionization is fast compared to internal dynamics. This can change when going to picosecond (ps) or even nanosecond (ns) pulses.

Using a fs laser system, PECD has been demonstrated[16,17] by employing 2+1 resonance-enhanced multi-photon ionization, where in those cases after two photons an electronic state has been excited and one further photon has ionized the system. This process is known as 2+1 REMPI. PECD provides the possibility to determine changes in enantiomeric excess (e.e.) down to the sub-one percent regime,[18–20] and its analytical capabilities have already been acknowledged.[4,21]

For REMPI studies, changing the laser wavelength allows to study the dependence of PECD on intermediate state and photoelectron kinetic energy[17,22–24] in comparison to theoretical descriptions.[25,26] The influence of polarization state used for excitation and ionization on observed PECD was modeled[26] and investigated experimentally.[27] Using a fs pump-probe setup, dynamics in the 3s intermediate state were investigated for fenchone.[28,29] When the duration of the laser pulses is increased to longer than ps, intra-molecular dynamics in addition to rotation of the molecules can evolve during ionization, where it is not clear whether PECD can be observed. Here, we report on observation of PECD on the ns timescale. When ns lasers are used, the lifetime of the intermediate states of fenchone is much shorter than the laser pulse duration. Ns lasers are widely used in analytical chemistry.[4,30] The ability to use an ordinary ns laser system to measure PECD furthermore reduces the technical requirements to use PECD in analytics.

[a] A. Kastner, T. Ring, Dr. H. Braun, Dr. A. Senftleben, Prof. Dr. T. Baumert
Institut für Physik und CINSaT
Universität Kassel, Heinrich-Plett-Strasse 40
34132 Kassel (Germany)
phone: +49 (0)561 804 4452
fax: +49 (0)561 804 4453
E-mail: tbaumert@uni-kassel.de

Supporting information for this article is available on the WWW under https://doi.org/10.1002/cphc.201900289

The three-photon excitation and ionization scheme for fenchone derived from a previous fs experiment[24] is depicted in Figure 1a). At least three different electronic intermediate states can be populated via two-photon excitation from the S_0 ground state, where the third photon ionizes the system. The first two intermediate states correspond to excitation of an electron from the HOMO leading to electronic intermediates having 3s and 3p Rydberg character as observed previously.[24,31,32] Assuming parallel potential energy surfaces, the ionization from Rydberg states to the cation does not change the vibrational quantum number v, which is called a $\Delta v = 0$ propensity rule. For the present ionization mechanism in fenchone this has been observed experimentally.[24] The third excitation is $\pi^* \leftarrow \sigma$ and was also observed experimentally.[24,31]

The experimental setup is depicted in Figure 1b). The results shown herein will be compared to a fs experiment with a spectrum encompassing the ns spectrum (see Figure 1c)). A detailed description of experimental methods can be found in the Supporting Information (SI). In brief, the ns laser pulses are guided to the VMI chamber and the polarization is converted into either left- or right circularly polarized using a quarter-wave plate (QWP). The laser pulses are focused into the VMI chamber and are intersected with an effusive gas beam of fenchone. The VMI images are analyzed by an expansion into Legendre polynomials, where the odd-order coefficients were weighted and linearly summed to obtain a PECD metric characterized by one number (LPECD).[33] One important point for application in analytical chemistry is the signal rate (yield per time). It turns out that the ns laser easily competes with the signal rate found in previous fs measurements.[18] Further details can be found in the SI.

In a previous fs experiment,[24] the absorption into different intermediate states showed a continuous evolution when scanning the excitation wavelength from 431 nm to 359 nm. At the longest wavelengths, only ionization via the 3s intermediate state was visible in the photoelectron spectra (PES). Below 393 nm, the 3p contribution appeared in addition. A third intermediate state, corresponding to a $\pi^* \leftarrow \sigma$ excitation, showed up in the PES below 363 nm. At the shortest wavelength of 359 nm we obtained the spectrum shown in Figure 2a). The PES contains three distinct contributions, which can

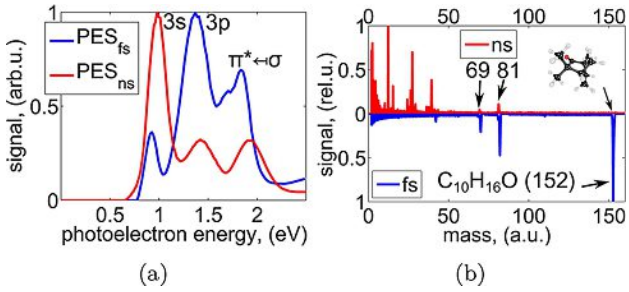

Figure 2. a) Comparison of photoelectron spectra obtained by ionizing (S)-(+)-fenchone either with the ns laser (red line) or with the fs laser (blue line). b) Ns mass spectrum (red) in comparison with a fs mass spectrum (blue).

be assigned to excitation of 3s ← n, 3p ← n and $\pi^* \leftarrow \sigma$ transitions.[24] The ns PES resembles the fs PES with respect to contributions and their energetic positions. Assuming the formerly observed $\Delta v = 0$ propensity rule, the photoelectron energy scales as $\hbar\omega$, where ω is the laser angular frequency. This deviates from a non-resonant excitation, where the scaling would be $3\hbar\omega$.[24] Please note that intra-molecular vibrational energy redistribution as formerly observed for fenchone on a few hundred fs timescale[28,29] may occur in the 3s Rydberg state. Due to the $\Delta v = 0$ propensity rule, the photoelectron energy is not affected by such effects. From the previously determined energies to excite the 3s and 3p states in their vibrational origins we can calculate the amount of vibrational excitation energy to be about 1.0 eV in the 3s and about 0.6 eV in the 3p states at the ns laser's 355 nm.

We now compare the energy values of the three peaks in the ns PES to those of the same contributions in the fs PES using Gaussian fit functions to determine the center of each peak. The differences between ns and fs are +56 meV for the 3s, +37 meV for the 3p and +86 meV for the $\pi^* \leftarrow \sigma$ contributions. For a 2+1 REMPI via the 3s and 3p Rydberg states, where the final ionization step does not change the vibrational quantum number, it has been shown[24] that a difference in the photon energy yields the same difference in the photoelectron energy.[24] Consequently, the change in the 3s and 3p peak positions agrees well with the increase in photon energy by +40 meV.

The most striking difference between the ns and fs PES are the relative heights of the individual contributions: While the 3s peak has the lowest intensity in the fs experiment, it dwarfs the other two lines in the ns PES. A reason for this change can be found in the different lifetimes of the intermediate states in the REMPI excitation and ionization scheme: Earlier works reported

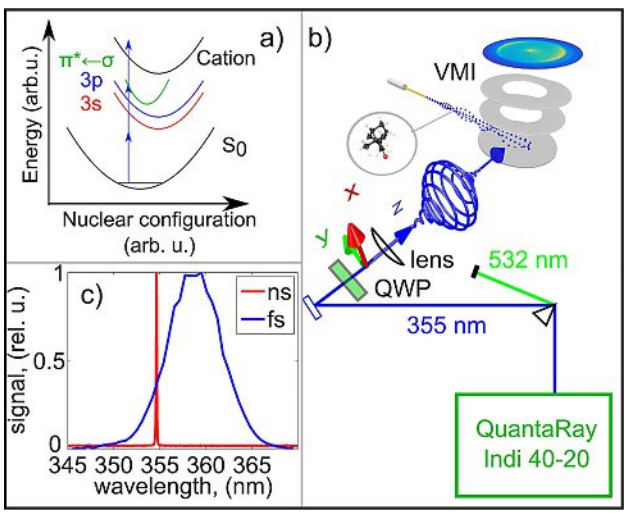

Figure 1. a) Schematic excitation and ionization scheme for the 2+1 resonantly enhanced multi-photon ionization (REMPI) observed in previous fs experiments. Three different intermediates are populated by two-photon excitation: 3s and 3p are Rydberg states of the neutral molecule, whereas $\pi^* \leftarrow \sigma$ is a valence-electron excitation. b) Experimental setup for the ns PECD experiment and c) comparison of ns and fs laser bandwidth spectra.

a ps lifetime for the 3s state[24,29] and an order of magnitude shorter lifetime for the 3p state.[24] As the fs pulses are much shorter than both lifetimes, decay of the intermediate state before the final ionization step will not be significant. However, in the ns case much more time can pass between excitation and ionization, such that the number of molecules available for ionization is affected by the lifetime of the intermediates. Therefore, the shorter lifetime of the 3p compared to the 3s reduces its relative contribution to the PES.

We now turn to discussion of the mass spectra. The mass spectrum for the ns ionization (shown in red in Figure 2b)) shows stronger fragmentation of the molecules as compared to the fs experiment (shown in blue). The fs mass spectrum is dominated by the parent ion, whereas in the ns mass spectrum mainly masses below 50 amu are present. The two heaviest fragments with masses 69 amu and 81 amu found in the ns mass spectrum can be found as well in the fs mass spectrum. In previous fs experiments, increasing the laser intensity has been found to lead to more fragmentation while the PECD has stayed basically unaffected.[33] This has been attributed to ionization preceding fragmentation in agreement with coincidence imaging findings.[17] In recent mass-tagging experiments on limonene,[22] barely different PECD values were observed on parent compared to fragment ionization. As ns and fs PES contain the same peaks and the shifts in peak positions can be explained by different center wavelengths, we presume that the ns PES stems mainly from parent ionization prior to ionic dissociation. As we show below, the ns LPECD values are similar compared to fs values. This hints to PECD being recorded from undissociated molecules.

A PECD image is formed by subtracting the photoelectron image on the detector for right circularly polarized (RCP) light from the image for left circularly polarized (LCP) light (see SI). In Figure 3 the anti-symmetric parts of the PECD images obtained for (S)-(+)- and (R)-(−)-fenchone are shown. The raw data is depicted in the upper half of the images, whereas the derived contribution of the odd-order Legendre polynomials is depicted in the lower half of the images. The strongest PECD-bearing contribution is the innermost ring, which comes from excitation of the 3s state. A detailed description of the data evaluation can be found in the SI. In brief, the Legendre coefficients and LPECD values are obtained by weighted averaging over the FWHM of each peak in the PES. In the fs experiment, two contributions to the 3p peak with opposite signs have been observed.[24] Here, only one contribution underneath the 3p peak is observed.

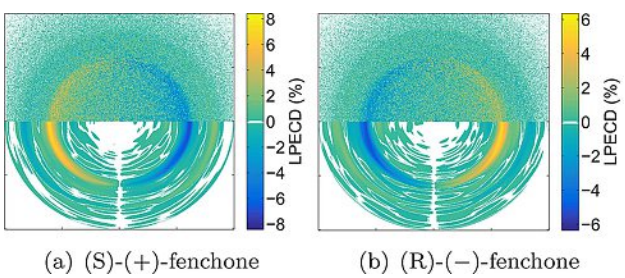

Figure 3. Anti-symmetrized PECD image for (S)-(+)-fenchone (a) and (R)-(−)-fenchone (b). The laser propagates from left to right in the images.

The resulting weighted average LPECD values are depicted in Figure 4a). Three different data sets each containing the values for the observed contributions to the PES are shown in Figure 4a). The two data sets on the left hand side are for both enantiomers of fenchone using the ns laser and the data set shown on the right hand side is data obtained with the fs laser for (S)-(+)-fenchone. Comparing the ns data, all the LPECD values are mirrored in sign when exchanging the enantiomer, while in magnitude they differ due to the different e.e. for the (R)-(−)-fenchone specimen (about 84% e.e.) compared to the (S)-(+)-fenchone specimen (about 99.9% e.e.).[18] Furthermore, for a given enantiomer the sign of LPECD for 3s and 3p is the same, but the sign changes for $\pi^* \leftarrow \sigma$.

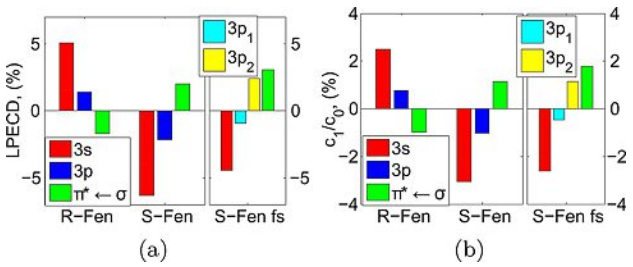

Figure 4. Comparison of weighted LPECD (a) and c_1/c_0 ratio of Legendre coefficients (b) values for the different intermediate resonances (color-coded) for (R)-(−)-fenchone and (S)-(+)-fenchone using the ns laser (left two data sets) and for comparison the values obtained for (S)-(+)-fenchone in a previous fs experiment (right side).

If we compare the ns PECD values obtained for (S)-(+)-fenchone to the ones found in the fs measurement, it can be seen that the magnitude and sign for the 3s as well as $\pi^* \leftarrow \sigma$ contribution is about the same. The value for 3p has the same sign as the $3p_1$ found in the fs experiment. In the fs experiment, the LPECD for $3p_2$ has a higher value and opposite sign compared to the $3p_1$ contribution. This could hint in the direction that several intra-molecular dynamics are launched when exciting the 3p manifold, especially in the energy region labeled $3p_2$ in the fs experiment.[24] However, further experimental and theoretical considerations are necessary to clarify this.

The dominant contributions to the LPECD metric stem from the c_1/c_0 coefficients in agreement with previous findings.[24] The c_1 values obtained for the different intermediate states for the ns and the fs experiment are plotted in Figure 4b) and show reasonable agreement. The higher order coefficients have much weaker influence on the LPECD and are about one order of magnitude smaller compared to the c_1 values and are therefore not displayed.

In this contribution, we demonstrated that PECD can be observed when using an ordinary ns Nd:YAG laser. In comparison to fs findings, the 3s state dominates the PES for the ns experiment attributed to its longer lifetime as compared to the

3p state. The observed LPECD value for the 3s state is in agreement with previous fs PECD values.

Being able to use a commercial ns laser to observe PECD furthermore reduces the technical requirements to apply PECD in analytical chemistry and thus paves the way for many new investigations in chiral recognition in the gas phase.

Acknowledgement

The authors thank H. G. Lee for many fruitful discussions. This work was supported by the Deutsche Forschungsgemeinschaft (DFG) within the Sonderforschungsbereich SFB-1319 'Extreme Light for Sensing and Driving Molecular Chirality – ELCH'

Conflict of Interest

The authors declare no conflict of interest.

Keywords: Circular dichroism · Chirality · Photoelectron spectroscopy · Femtochemistry · Laser chemistry

[1] S. R. Domingos, C. Pérez, M. Schnell, *Annu. Rev. Phys. Chem.* **2018**, *69*, 499–519.
[2] M. Pitzer, R. Berger, J. Stohner, R. Dörner, M. Schöffler, *Chimia* **2018**, *72*, 384–388.
[3] D. Baykusheva, H. J. Wörner, *Phys. Rev. X* **2018**, *8*, 031060.
[4] U. Boesl, A. Kartouzian, *Annu. Rev. Anal. Chem.* **2016**, *9*, 343–364.
[5] B. Ritchie, *Phys. Rev. A* **1976**, *13*, 1411–1415.
[6] N. Böwering, T. Lischke, B. Schmidtke, N. Müller, T. Khalil, U. Heinzmann, *Phys. Rev. Lett.* **2001**, *86*, 1187–1190.
[7] I. Powis, *Adv. Chem. Phys.* **2008**, *138*, 267–329.
[8] H. Ganjitabar, R. Hadidi, G. A. Garcia, L. Nahon, I. Powis, *J. Mol. Spectrosc.* **2018**, *353*, 11–19.
[9] G. A. Garcia, L. Nahon, S. Daly, I. Powis, *Nat. Commun.* **2013**, *4*, 2132.
[10] I. Dreissigacker, M. Lein, *Phys. Rev. A* **2014**, *89*, 053406.
[11] D. W. Chandler, P. L. Houston, D. H. Parker, *J. Chem. Phys.* **2017**, *147*, 013601.
[12] J. Miles, D. Fernandes, A. Young, C. M. M. Bond, S. W. Crane, O. Ghafur, D. Townsend, J. Sá, J. B. Greenwood, *Anal. Chim. Acta* **2017**, *984*, 134–139.
[13] L. Nahon, G. A. Garcia, I. Powis, *J. Electron Spectrosc. Relat. Phenom.* **2015**, *204*, 322–334.
[14] S. Turchini, *J. Phys. Condens. Matter* **2017**, *29*, 503001.
[15] R. Hadidi, D. K. Bozanic, G. A. Garcia, L. Nahon, *Adv. Phys.* **2018**, *3*, 834–861.
[16] C. Lux, M. Wollenhaupt, T. Bolze, Q. Liang, J. Köhler, C. Sarpe, T. Baumert, *Angew. Chem. Int. Ed.* **2012**, *51*, 5001–5005; *Angew. Chem.* **2012**, *124*, 5086–5090.
[17] C. S. Lehmann, N. Bhargava Ram, I. Powis, M. H. M. Janssen, *J. Chem. Phys.* **2013**, *139*, 234307.
[18] A. Kastner, C. Lux, T. Ring, S. Züllighoven, C. Sarpe, A. Senftleben, T. Baumert, *ChemPhysChem* **2016**, *17*, 1119–1122.
[19] L. Nahon, L. Nag, G. A. Garcia, I. Myrgorodska, U. Meierhenrich, S. Beaulieu, V. Wanie, V. Blanchet, R. Géneaux, I. Powis, *Phys. Chem. Chem. Phys.*, **2016**, *18*, 12696–12706.
[20] A. Comby, E. Bloch, C. M. M. Bond, Descamps, J. Miles, S. Petit, S. Rozen, J. B. Greenwood, V. Blanchet, Y. Mairesse, *Nat. Commun.* **2018**, *9*, 5212.
[21] M. H. M. Janssen, I. Powis, *Spectroscopy Online* **2017**, *15*, 16–23.
[22] M. M. Rafie Fanood, M. H. M. Janssen, I. Powis, *J. Chem. Phys.*, **2016** *145*, 124320.
[23] S. Beaulieu, A. Ferré, R. Géneaux, R. Canonge, D. Descamps, B. Fabre, N. Fedorov, F. Légaré, S. Petit, T. Ruchon, V. Blanchet, Y. Mairesse, B. Pons, *New J. Phys.* **2016**, *18*, 102002.
[24] A. Kastner, T. Ring, B. C. Krüger, G. B. Park, T. Schäfer, A. Senftleben, T. Baumert, *J. Chem. Phys.* **2017**, *147*, 013926.
[25] A. D. Müller, A. N. Artemyev, P. V. Demekhin, *J. Chem. Phys.* **2018**, *148*, 214307.
[26] R. E. Goetz, T. A. Isaev, B. Nikoobakht, R. Berger, C. P. Koch, *J. Chem. Phys.* **2017**, *146*, 24306.
[27] S. Beaulieu, A. Comby, D. Descamps, S. Petit, F. Légaré, B. Fabre, V. Blanchet, Y. Mairesse, *J. Chem. Phys.* **2018**, *149*, 134301.
[28] S. Beaulieu, A. Comby, B. Fabre, D. Descamps, A. Ferré, G. Garcia, R. Géneaux, F. Légaré, L. Nahon, S. Petit, T. Ruchon, B. Pons, V. Blanchet, Y. Mairesse, *Faraday Discuss.* **2016**, *194*, 325–348.
[29] A. Comby, S. Beaulieu, M. Boggio-Pasqua, D. Descamps, F. Légaré, L. Nahon, S. Petit, B. Pons, B. Fabre, Y. Mairesse, V. Blanchet, *J. Phys. Chem. Lett.* **2016**, *7*, 4514–4519.
[30] R. E. Russo, X. Mao, H. Liu, J. Gonzalez, S. S. Mao, *Talanta* **2002**, *57*, 425–451.
[31] F. Pulm, J. Schram, S. Grimme, S. Peyerimhoff, *Chem. Phys.* **1997**, *224*, 143–155.
[32] J. W. Driscoll, T. Baer, T. J. Cornish, *J. Mol. Struct.* **1991**, *249*, 95–107.
[33] C. Lux, M. Wollenhaupt, C. Sarpe, T. Baumert, *ChemPhysChem* **2015**, *16*, 115–137.

Manuscript received: March 21, 2019
Revised manuscript received: April 2, 2019
Accepted manuscript online: April 11, 2019
Version of record online: May 9, 2019

CHEMPHYSCHEM

Supporting Information

Observation of Photoelectron Circular Dichroism Using a Nanosecond Laser

Alexander Kastner, Tom Ring, Hendrike Braun, Arne Senftleben, and Thomas Baumert*

-Supporting Information-

April 1, 2019

Herein, a detailed description of the experimental methods in the first section as well as additional details concerning the derivation of the weighted average LPECD values are shown in section two.

1 Experimental setup

The experimental setup is depicted in figure 1 b) in the main text. The output of a Nd:YAG laser (*Spectra Physics QuantaRay INDI 40-20*) is frequency-tripled (to 355 nm). At a repetition rate of 20 Hz, the pulses have about 6 ns temporal width and a maximum pulse energy of about 70 mJ, where about 2 mJ were used in the experiment. An important point for application in analytics is the signal rate (yield per time). In previous fs experiments, about 50 molecules per laser shot were ionized[1] leading to a rate of about $10^{4.7\pm0.5}$ ionization events per second. A similar derivation for the ns laser leads to a signal rate of about $10^{5.5\pm0.5}$ ionization events per second and thereby the ns laser can easily compete with the fs laser. The average laser powers used were about 40 mW for the ns laser and about 3 mW for the fs laser.

The output of the Nd:YAG laser is guided through a UV-grade fused silica prism to spatially separate the 355 nm from the remaining 532 nm light. The laser spectrum of the Nd:YAG as measured directly in front of the VMI chamber by a spectrometer (*Avantes AvaSpec 3648*, wavelength region 320–880 nm, wavelength resolution $\sim$ 0.15 nm) contains only a peak at about 355 nm (shown in figure 1 c) in the main text). The laser spectrum of the femtosecond laser (blue) was measured by a similar spectrometer (*Avantes AvaSpec 2048*, wavelength resolution $\sim$ 0.55 nm) and is plotted for comparison in figure 1 c) in the main text. It can be seen that the broad femtosecond laser spectrum encompasses the Nd:YAG's wavelength.

The Nd:YAG laser beam is guided to the VMI chamber using high-reflective mirrors for 355 nm. In front of the VMI chamber the laser beam is horizontally polarized. An achromatic quarter-wave plate (QWP, *B.Halle*) was used to convert linearly polarized (LIN) to left circularly polarized (LCP) or right circularly polarized light (RCP). The quality of polarization is determined using a Glan-Laser polarizer (*ThorLabs GL10*) and a powermeter (*Ophir Nova II*).

The Stokes $|S_3|$ parameter that grades the circularity of the polarization is about 99.9 % for LCP and 99.8 % for the RCP setting. No correction of the experimental data with respect to the $|S_3|$ value is done.

The laser beam is focused into the interaction region of the VMI spectrometer by an $f = 200$ mm plano-convex UV-grade fused silica lens. The laser beam

is intersected with an effusive gas beam of the substances. The VMI setup is similar to previous experiments,[2, 3] although the VMI plates have been replaced resulting in slightly better energy resolution of about $\Delta E/E \approx 4\%$ as measured at the lower spin-orbit state of xenon ($^2P_{3/2}$). Energy calibration of the VMI is done using the 355 nm output of the Nd:YAG driving four-photon ionization of xenon.

The VMI can be used to either project photoelectrons or photoions onto an imaging detector comprising a double-stack MCP assembly in Chevron configuration and a phosphor screen (*SI-Instruments GmbH*). In photoelectron detection mode, the three-dimensional photelectron momentum distribution is projected onto the two-dimensional detector such that the electrons' momentum vector components lateral to the spectrometer axis (x-axis) are measured. The absolute value of the momentum vector is mapped to radial position on the detector. The projected photoelectron momentum distributions are recorded using a 1.4 million pixel CCD camera (12 bit, *Lumenera Lw165m*). The VMI plate voltages were set to image photoelectrons with kinetic energies up to about 4.2 eV onto the detector. Alternatively, ion time-of-flight mass spectra can be recorded on an oscilloscope (*LeCroy Waverunner 640Zi*) via a capacitively coupled output.

In total, about 40000 laser pulses were used equally distributed over LCP and RCP measurements, where every about 1300 laser pulses the circularity is switched between LCP and RCP to reduce the effect of slow experimental fluctuations. The PECD image is calculated by subtracting the RCP photoelectron momentum distribution image from the LCP photoelectron momentum distribution image. From these images, a quantification of PECD, denoted as LPECD, can be derived by subtracting the integral over backward hemisphere of the PECD image from the integral over the forward hemisphere and normalizing the result by the total signal obtained with LCP and RCP light. Effectively, this measure contains only the anti-symmetric part of the PECD image.[2] Therefore, a way to visually isolate the chiral contribution to PECD images is to anti-symmetrize them, which has been done in the upper halves of images 3 (a) and (b) in the main text.

The original three-dimensional photoelectron momentum distribution is reconstructed using an Abel inversion routine via the pBasex algorithm.[2, 4] pBasex expands the angular distribution for every photoelectron momentum into a series of Legendre polynomials. Following Yang's theorem,[5] the series is truncated after the 8^{th} order. Using the pBasex algorithm, different contributions in the photoelectron spectrum can be evaluated separately. The pBasex evaluation here is similar to the previous one,[2] although the radial sampling point number has been doubled to a value of 200. The chiral signature is contained in the anti-symmetric Legendre polynomials, i.e. the odd-order coefficients. The magnitude of PECD can be derived by computing a sum over the odd-order coefficients c_i contributions normalized to the total signal c_0, denoted as LPECD:[2]

$$\text{LPECD} = \frac{1}{c_0}\left(2c_1 - \frac{1}{2}c_3 + \frac{1}{4}c_5 - \frac{5}{32}c_7\right). \tag{1}$$

If only a single peak in the photoelectron spectrum c_0 is observed, the LPECD metric and the coefficients are derived using a weighted average over the full width at half maximum (FWHM) of the peak. If multiple peaks are

observed in the photoelectron spectrum, the weighted average is performed for each peak separately to derive the weighted average values.

The enantiopure (S)-(+)- and (R)-(−)-fenchone samples were purchased from Sigma-Aldrich with a specified constitutional purity of 99.2 % and used without further purification. The enantiomeric excess (e.e.) as measured by gas chromatography was 99.9 % for (S)-(+)-fenchone and 84 % for (R)-(−)-fenchone.[1]

2 Extracting peak-averaged LPECD and coefficient values

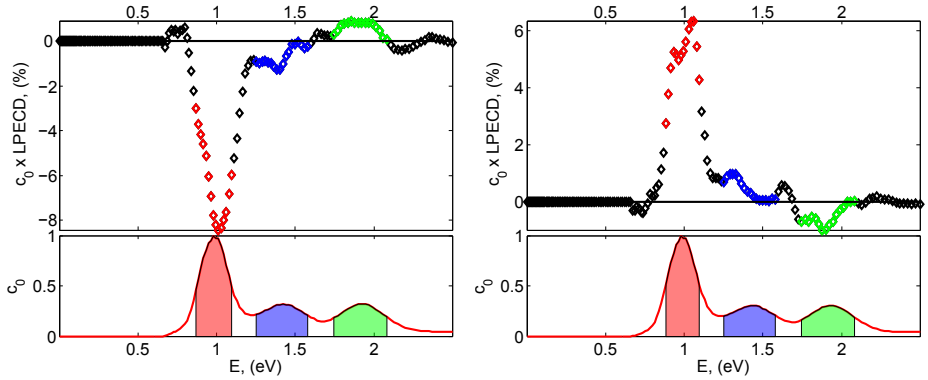

(a) (S)-(+)-fenchone (b) (R)-(−)-fenchone

Figure S 1. $c_0 \times$ LPECD curves (upper half of plots) and c_0 (lower half of plots) shown for (S)-(+) (a) and (R)-(−)-fenchone (b). The points inside the FWHM of each peak in the $c_0 \times$LPECD curve are colored and the corresponding area underneath the c_0 curve is shaded for better visibility.

The PECD evaluation has been done as described in previous work,[3] where the derived coefficients and LPECD values are obtained by weighted averaging over the FWHM width of each peak in the c_0 curve. To derive the FWHM width for each peak separately, a Gaussian was fitted each to the 3s, 3p and $\pi^* \leftarrow \sigma$ peak observed in the c_0 curve. For all three contributions in the photoelectron spectrum, the $c_0 \times$ LPECD shows no sign change in the region of FWHM of c_0. In the fs experiment, two contributions to the $c_0 \times$ LPECD curve with opposite signs have been observed underneath the 3p peak.[3] Here, only one contribution underneath the 3p peak seems to be present. Therefore, the 3p peak is evaluated the same way as the 3s and the $\pi^* \leftarrow \sigma$ by fitting a single Gaussian. To derive the LPECD and coefficient values, weighted averaging within the FWHM of each peak is done.

The comparison between nanosecond and femtosecond LPECD and coefficient data is shown in the main text. The femtosecond data was re-evaluated using 200 radial sampling points leading to barely altered LPECD values compared to previous findings.[3]

References

[1] A. Kastner, C. Lux, T. Ring, S. Züllighoven, C. Sarpe, A. Senftleben, and T. Baumert, *ChemPhysChem*, **2016**, 17, 1119-1122.

[2] C. Lux, M. Wollenhaupt, C. Sarpe, and T. Baumert, *ChemPhysChem*, **2015**, 16, 115-137.

[3] A. Kastner, T. Ring, B. C. Krüger, G. B. Park, T. Schäfer, A. Senftleben, and T. Baumert, *The Journal of Chemical Physics*, **2017**, 147, 013926.

[4] G. A. Garcia, L. Nahon, and I. Powis, *Review of Scientific Instruments*, **2004**, 75(11), 4989-4996.

[5] C. N. Yang, Physical Review, **1948**, 74, 764-772.